TWELFTH EUROPEAN ROTORCRAFT FORUM

Paper No. 82

VALIDATION OF A METHOD FOR AIR RESONANCE TESTING OF HELICOPTERS AT MODEL SCALE USING ACTIVE CONTROL OF PYLON DYNAMIC CHARACTERISTICS

Richard L. Bielawa

Rotorcraft Technology Center
Department of Mechanical Engineering,
Aeronautical Engineering and Mechanics,
Rensselaer Polytechnic Institute
Troy, New York 12180-3590 U.S.A.

September 22 - 25, 1986

Garmisch-Partenkirchen
Federal Republic of Germany

Deutsche Gesellschaft für Luft- und Raumfahrt e. V. (DGLR)
Godesberger Allee 70, D-5300 Bonn 2, F.R.G.

VALIDATION OF A METHOD FOR AIR RESONANCE TESTING OF HELICOPTERS AT MODEL SCALE USING ACTIVE CONTROL OF PYLON DYNAMIC CHARACTERISTICS*

by

Richard L. Bielawa
Associate Professor
Department of Mechanical Engineering,
Aeronautical Engineering and Mechanics
Rensselaer Polytechnic Institute
Troy, New York 12180-3590, USA

Abstract

A basic problem inherent in the testing for helicopter air resonance at model scale is the design and fabrication of the pylon support structure to effect both a proper (Froude) scaling and adequate variability of the pylon parameters. Generally, provision for suitable pylon parameter variability (especially the inertias) within a properly scaled configuration is often difficult at best using passive properties. One method of overcoming this difficulty is to provide for active control of the pylon properties. This is potentially achievable using suitably controlled hydraulic feedback servo actuators acting in response to the measured motion of the pylon. The objective of the present study is to investigate the validity of such an approach using analytical means. The results presented compare the air resonance eigensolutions obtained for a full-scale free-flying helicopter to those obtained for various approximations inherent in such a method of model testing. Analytical formulations are presented describing the modifications required of a basic air resonance theory to account for the dynamics of the selected feedback control network.

1. Introduction

1.1 Background

Despite the growing sophistication of analyses for helicopter air resonance, stability tests are still undertaken in the development of new hingeless and bearingless rotor helicopter designs as the principal confirmation that such designs are indeed stable. Air resonance stability tests are typically performed at model scale for a variety of reasons: cost, safety of flight, parametric variability, timeliness of results to impact on the design, etc. Presently, model tests are usually performed with a model having rotor blades which are appropriately designed to have full-scale Lock (inertia) and Froude numbers, and a pylon (airframe) which preserves the rotor mass to pylon mass ratio.

*Presented at the 12th European Rotorcraft Forum, 22-25 September 1986, Garmisch-Partenkirchen, Germany.

The requirement for both inertia and Froude scaling, the available techniques for lightweight, low-damping model construction and the need to approximate free-flight with a constrained non-flying pylon in a wind tunnel environment all invariably drive the model design to the same simplified pylon configuration: The pylon system is typically designed for articulation only in pitch and roll about some effective total aircraft center-of-gravity point using a gimbal arangement, as shown below:

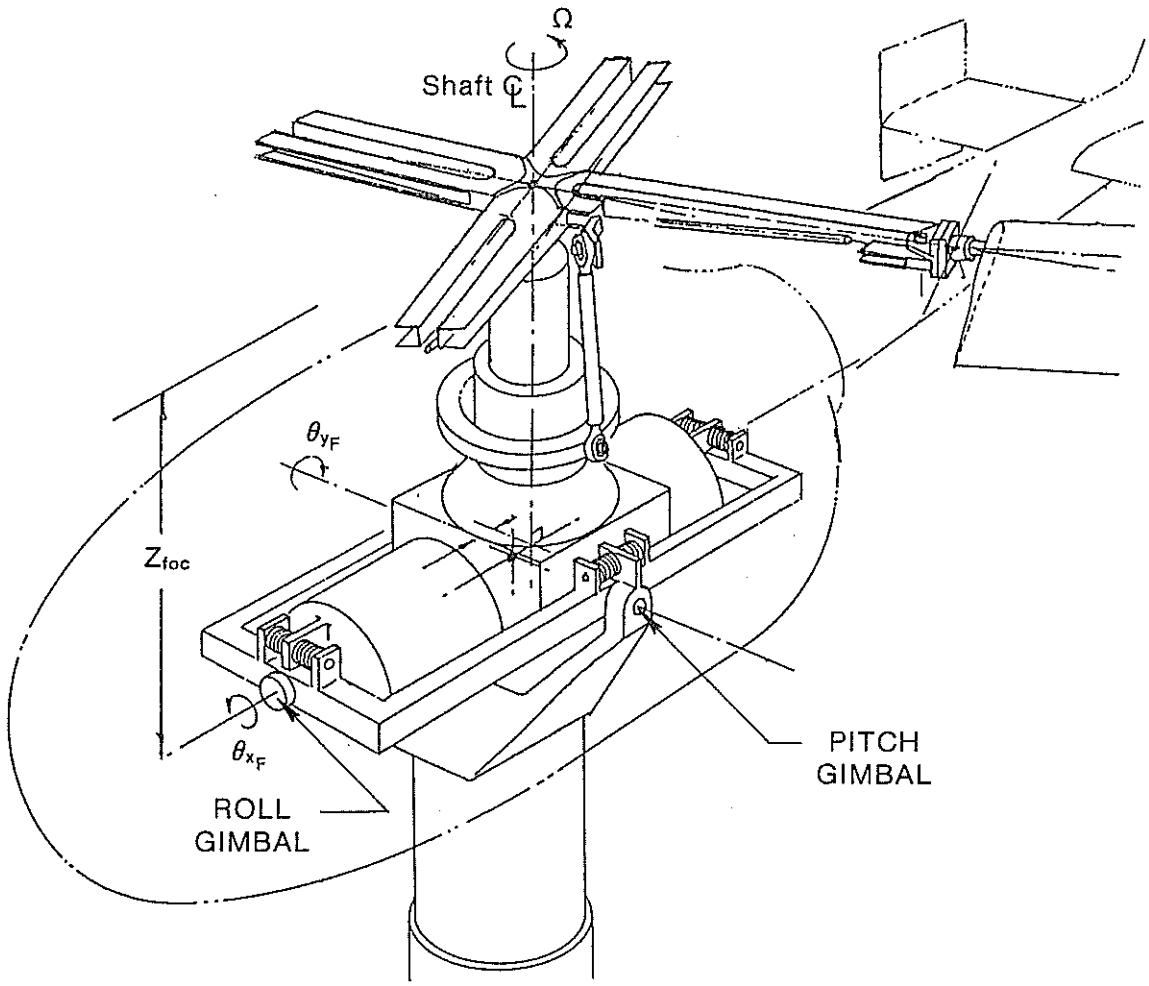

Figure 1. Schematic of a 1/5.86 Scale BMR/BO-105 Air Resonance Model (Ref. 1)

References 1 and 2 present results obtained with this basic type of model configuration. The design and construction of such a configuration, with a scaling of its dynamics as close to that of the full-scale vehicle as possible, represents a substantial accomplishment both in engineering and craftsmanship.

The intrinsic deficiences and/or difficulties in this approach, however, are that:

(1) The modeling of the pylon mass as a gimbaled rigid body mass articulated in pitch and roll about some effective center-of-gravity point is an approximation subject to inaccuracies (Ref. 3).

(2) Some ranges in pylon parameters may be simply impractical to construct at model scale. This difficulty is compounded by the fact that relative internal damping tends to vary in a inverse manner with model scale.

(3) The need to approximate the gravity springs in pitch and roll, together with the need to approximate free-flight trim conditions, places constraints on both the elastic restraints and preloads about the gimbal. For some combinations of required spring rates and preloads special gadgetry may be either impractical or too expensive.

1.2 Active Control of Pylon Characteristics

One method of alleviating at least the second and third of the above identified deficiencies is to provide the pylon structure of the rotor test rig with an active control system such that arbitrary force-response relationships as seen by the rotor can be closely approximated. Such an approach inherently provides the wherewithal for achieving the required spring rates and preloads about the gimbal. The present work is a validation analysis of a design of such a model test configuration currently under development with the Sikorsky Aircraft Division of United Technologies. Because of the preliminary status of this development an optimal selection of dynamic parameters was not available and those included in the analysis were therefore taken as a given.

The starting point for a proper mathematical simulation of this configuration is a description of the physical components of the model test rig. As seen in Figure 2., the pylon in this case is a gimbaled mass consisting of the rotor shaft and its bearing package (denoted as part A), the attached swash-plate assembly (not shown for clarity), the rotor hub and the outer gimbal ring (denoted as part B). In addition to the more or less conventional gimbaling in pitch and roll the pylon mass is additionally configured to have a heave degree-of-freedom. Thus, the pylon mass also includes the outer frame part (denoted as part C).

The figure indicates a flexible coupling of the rotor shaft to the drive shaft. Such a coupling is intended to provide a high degree of compliance not only in rotation about the pitch and roll axes, but in axial extension as well. Thus, the gimbaled mass has a high degree of articulation and is in of itself statically unstable. The pylon mass is then supported and driven

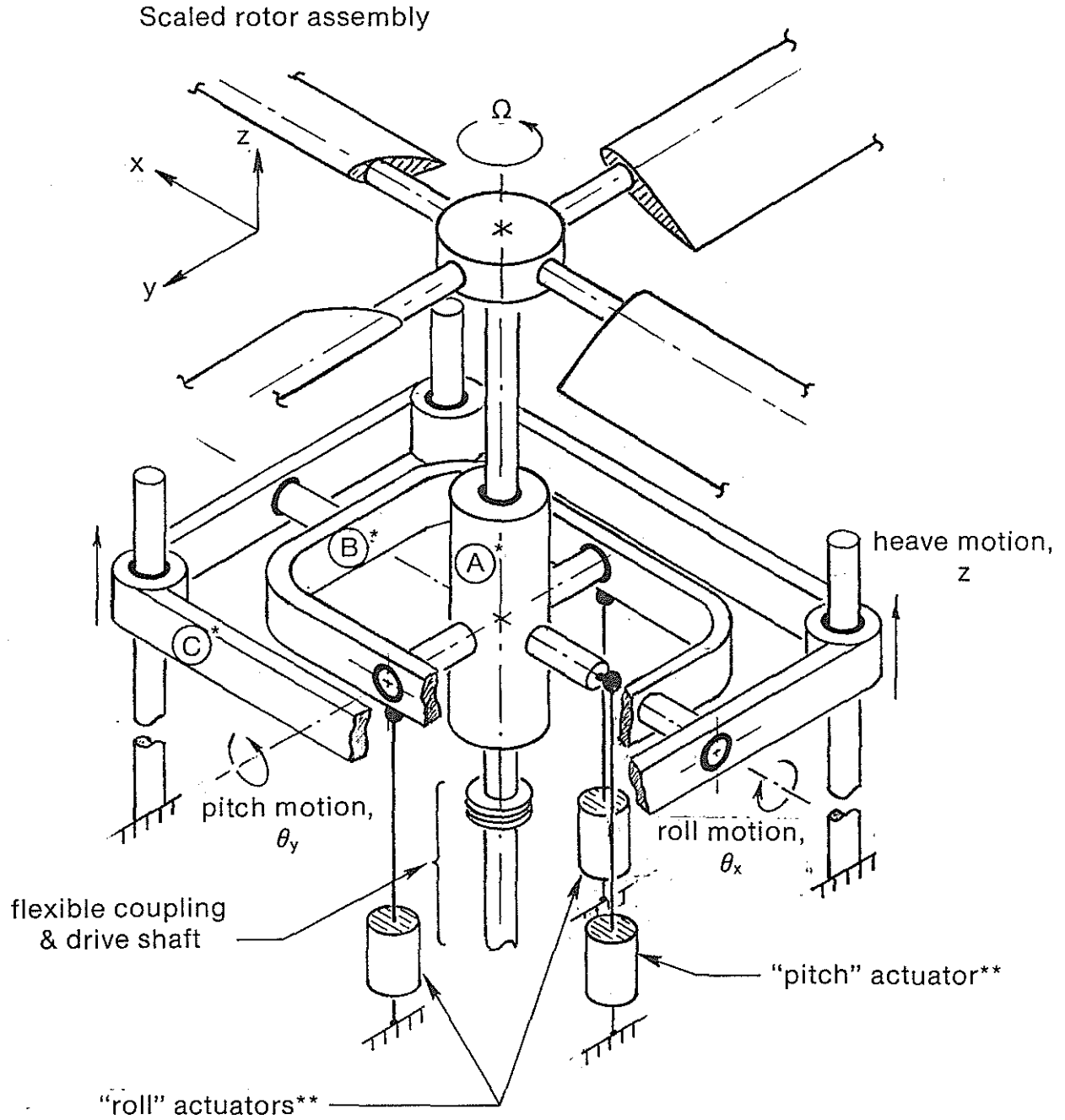

* Parts Ⓐ, Ⓑ, and Ⓒ comprise the actual non-scaled rig pylon assembly.

** All three actuators are needed for modification of the heave and pitch dynamic characteristics.

Figure 2. Schematic of Model Helicopter Test Rig with Active Control of Pylon Dynamic Characteristics

dynamically by the three attached hydraulic actuators which are linked to a structural ground point. the actuators are nonpolar symmetrically located around the rotor axis in a manner similar to a conventional swash-plate installation. Thus, the pylon mass is constained to have only three degrees-of-freedom: alternatively, heave, pitch and roll, or the vertical displacements of the three actuator attachment points, z_1, z_2 and z_3.

Each of the actuators is in turn controlled by an appropriate feedback network. The error signals which drive these networks are the measured responses (displacements, velocities and accelerations) together with other appropriate feedback quantities.

1.3 Scope of Validation Study

This form of testing does not address the first of the above identified inherent deficiencies and necessarily introduces additional dynamics associated with the active controller. Furthermore, an additional constraint, to be applied to initial tests using this test methodology is the use of a "mixed scaling" procedure wherein the velocity scaling, λ_V, has a value other than that dictated by a strict Froude number scaling ($= \sqrt{\lambda_\ell}$, where λ_ℓ is the length scale factor).

In light of these possible sources of inaccuracy a systematic validation of this form of air resonance test methodology was warranted.

The prime objective of the study was to explore the effects of (1) the gimbal constraint, (2) the feedback network, and (3) the use of an inexact Froude scaling, as they all relate to the accuracy of modeling the scaled air resonance phenomenon.

For the purpose of making an experimental validation, an exact modeling of the air resonance phenomenon is not critical in that we seek only to make comparisons between various approximations to the real world full-scale configuration. For this reason a relatively simple linear eigenvalue analysis was used as a basis. The study essentially consists of eigenvalue formulations of ever increasing dynamic complexity, leading eventually to an analysis of the complete configuration including the active feedback control network. The key dynamic parameter selected as the criterion for evaluating the various approximations is the real part of the air resonance eigenvalue, as nondimensionalized with respect to a (reference) rotor frequency, σ/Ω_{ref}.

It should be stressed that the present study relates only to a validation of the concept and correspondingly makes some idealizations with respect to the various components. Thus, the effects of the higher order dynamics residing in the transducers and servos, the presence of nonlinearities etc., are necessarily beyond the scope of the study.

To this end, a basic full-scale helicopter configuration was first taken as a starting point and analyzed for air resonance stability using an extension of the theory of Reference 4. The degree of model testing approximation was gradually increased by going next to a Froude scaled free-flying and then gimbal constrained configuration. The effects of a mixed scaling configuration were assessed for the gimbal constraint condition, and then for the bare actual rotor test rig with completely non-scaled properties.

The dynamic equations of motion representing the control feedback network were then coupled with the basic air resonance equations to form an expanded eigenproblem. Finally, analyses of the rig together with various combinations of incremental pylon characteristics feedback as well as other parameter variations were made. This paper presents the results of this analytical study and includes first, a description of the modifications to the basic air resonance theory to account for the dynamics of the feedback control network, and second, results of the parameter variations made with the resulting eigenanalysis.

2. Theoretical Development

2.1 Modification of Basic Air Resonance Equations

The basic equations of motion for air resonance given in Reference 4 were used as a starting point. To accommodate the need to assess the stability of a model in a wind tunnel environment vis-a-vis that in forward free-flight and because the test rig design is configured with a hub heave degree-of-freedom, z_F, this degree-of-freedom was added to the analysis. Additionally, provision was made for the direct application of external (generalized) forces and/or moments, as appropriate, to the five hub degrees-of-freedom. The principal features of the basic equations of motion resulting from this additional degree-of-freedom are given in the appendix.

The need to constrain the configuration from a free-flying one to one which is gimbal constrained, and the need to translate the three actuator forces to appropriate generalized forces for the three hub degrees-of-freedom (resulting from the gimbaling constraint) requires the use of displacement and force transformation matrices:

displacement constraint matrix due to gimbaling - The following matrix equation relates the unconstrained (hub) degrees-of-freedom to the constrained ones for gimbaling about a point, located a distance, z_{foc}, below the hub:

$$\begin{Bmatrix} x_F/R \\ y_F/R \\ \theta_{x_F} \\ \theta_{y_F} \\ z_F/R \end{Bmatrix} = \begin{bmatrix} 0 & z_{foc}/R & 0 \\ -z_{foc}/R & 0 & 0 \\ 1 & 0 & 0 \\ 0 & 1 & 0 \\ 0 & 0 & 1 \end{bmatrix} \begin{Bmatrix} \theta_{x_F} \\ \theta_{y_F} \\ z_F/R \end{Bmatrix} \qquad (1)$$

displacement and force resolution matrix for servo actuators - The displacements of the points where the servo actuators attach to the bearing housing portion of the shaft support must be related to the degrees-of-freedom selected to define the hub motion. Likewise, the actuator loads at these attachment points must be resolved into generalized forces appropriate to these degrees-of-freedom. Using Figure 3 as a guide, the following relationships can be formed:

$$\begin{Bmatrix} z_1 \\ z_2 \\ z_3 \end{Bmatrix} = \underbrace{\begin{bmatrix} 0 & x_a & R \\ -y_a & 0 & R \\ y_a & 0 & R \end{bmatrix}}_{= [\,T_2\,]} \begin{Bmatrix} \theta_{x_F} \\ \theta_{y_F} \\ z_F/R \end{Bmatrix} \qquad (2)$$

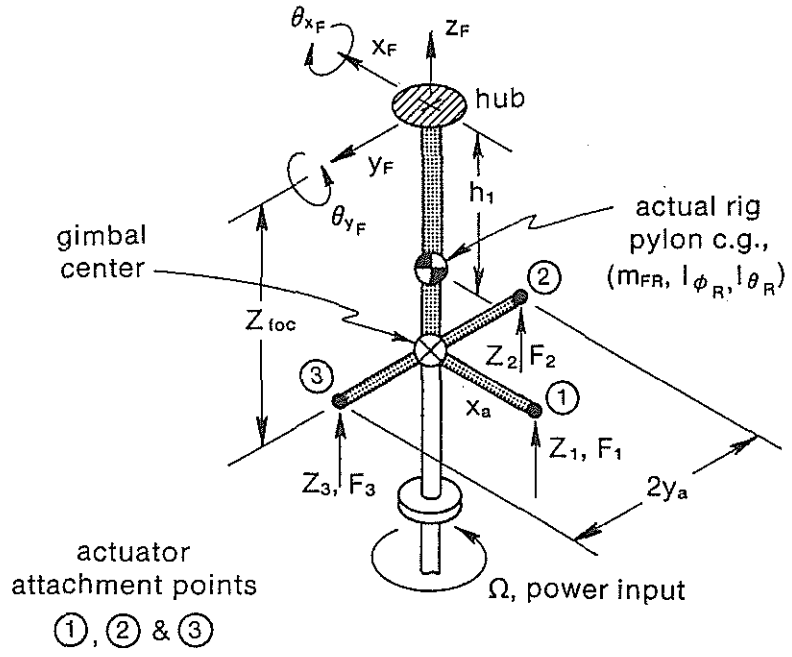

Figure 3. Kinematics of actuator attachment points

Similarly:

$$\begin{Bmatrix} F_1 \\ F_2 \\ F_3 \end{Bmatrix} = \underbrace{\begin{bmatrix} 0 & 1/x_a & 0 \\ -1/2y_a & -1/2x_a & 1/2R \\ 1/2y_a & -1/2x_a & 1/2R \end{bmatrix}}_{= [\,T_1\,]} \begin{Bmatrix} M_x^{(h)} \\ M_y^{(h)} \\ F_z^{(h)}{}_R \end{Bmatrix} \qquad (3)$$

Note that:

$$[\,T_1\,]^T = [\,T_2\,]^{-1} \qquad (4)$$

<u>body axes vs. wind tunnel axes</u> - Differences arise in the expressions for both the body inertia loads and the blade aerodynamic loads depending on whether the fuselage is in a (forward) free-flight condition or a gimbal constrained wind tunnel. The differences arise with respect to pitching motions in combination with forward flight velocity. In free-flight the vertical acceleration is measured in the body axis coordinate system and a substantial time derivative must be taken:

$$\frac{D^2 z_F}{Dt^2} = \ddot{z}_F + V \dot{\theta}_{y_F}$$

For the case of a gimbal mounted fuselage in a wind tunnel, the substantial time derivative does not apply and the second term would thus be omitted.

On the other hand, for the gimbal mounted wind tunnel case, the blade airload distribution would have an additional term due to the component of U_p arising from tunnel speed and pitch angle:

$$U_p = \cdots + V \theta_{y_F} + \cdots ,$$

This term is not present for the free-flight case.

2.2 <u>Feedback Network</u>

The basic idea of providing active control of the pylon dynamic characteristics is to drive the actuators as shown in Figure 2, with error signals which are proportional to the specified changes in the inertia, damping and/or stiffness forces experienced by the pylon. Thus, the most important feedback quantities are the accelerations, velocities and displacements of the

gimballed pylon mass (typically comprised of the bearing package, the attached swash-plate assembly, and the outer gimbal ring).

In addition to the basic feedback signal (for modification of the pylon characteristics) a secondary feedback loop was established for purposes of centering the pylon mass on the three force actuators and taking out the trim loads. Preliminary studies of the test rig using standard control theory (Ref. 5, e.g.) showed that the use of such a type of feedback could potentially lead to instabilities in the feedback loop itself. Consequently, additional transfer functions within this feedback loop were established for stabilization and other operational reasons to be addressed later. Figure 4 below presents the block diagram of the final feedback configuration with key details defined for one (typical) feedback loop structure driving one of the servo actuators:

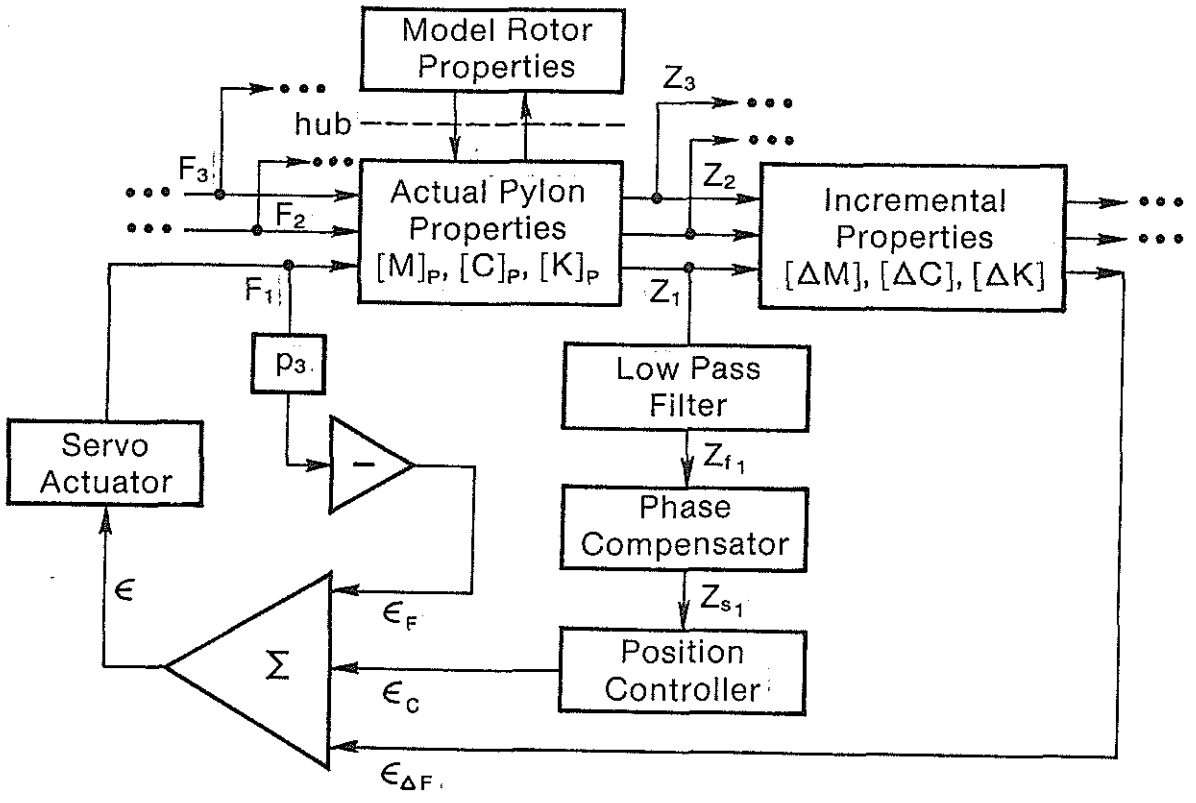

Figure 4. Block Diagram for the Servo Actuator Controlled Pylon Model Test Rig Showing a Typical Feedback Loop Network

The following features of this feedback loop network are to be noted:

primary feedback loop and interaction of the channels - The actual pylon properties are typically expressed in the form of inertia, damping and stiffness matrices. Consequently, as seen in above Equs. (2) and (3), one effect of the actuator kinematics is to couple the three actuator forces in producing all three generalized excitations appropriate to the pylon. Likewise, the responses of the degrees-of-freedom characteristic of the pylon produce coupling in the actuator attachment point degrees-of-freedom. Each of the incremental pylon force feedback signals is therefore linearly comprised of contributions from all of the measured attachment point degree-of-freedom response quantities, $\ddot{z}_j$, $\dot{z}_j$, and z_j (j = 1, 2, 3). This feedback signal we denote the "primary" feedback signal. Thus, the three component primary feedback error, $\{\epsilon_i\}_{\Delta F}$, can be formed by the following expression:

$$\{\epsilon_i\}_{\Delta F} = [T_1] \left[[\Delta M][T_1]^T\{\ddot{z}_j\} + [\Delta C][T_1]^T\{\dot{z}_j\} + [\Delta K][T_1]^T\{z_j\} \right] \tag{5}$$

where the incremental matrices, [ΔM], [ΔC] and [ΔK] represent the differences between the pylon dynamic properties to be simulated, $(\ )_s$, and those of the actual test rig, $(\ )_r$. Other than the coupling arising from these interactions, however, the three channels are completely uncoupled from each other.

low pass filtering and secondary feedback loops - As described above, one of the difficulties in testing dynamic rotor models with gimbal supports is the requirement to trim out the steady hub loads. Stated another way, for all test conditions, the gimbal rotations and, in the present case, the vertical position, all need to be centered. This is the primary function of the second feedback loop. Since the centering function is essentially a low frequency operation, a low pass filter is appropriate as a preconditioner for the position controller.

These two functions are governed by the following differential equations which respectively represent their feedback transfer functions for the ith servo feedback network:

low pass filter:

$$Q_3 \ddot{z}_{f_i} + Q_1 \dot{z}_{f_i} + Q_2 z_{f_i} - z_i = 0 \tag{6}$$

position controller:

$$p\left[z_{s_i} + a\dot{z}_{s_i} + b\int_0^t z_{s_i}\,dt\right] + \epsilon_{C_i} = 0 \qquad (7)$$

phase compensator:

In the initial development of the controller design this secondary feedback loop consisted of only the above two transfer functions. Subsequently, it was found that the the loop could potentially become unstable for filter and position controller coefficients needed for adequate centering action. An additional transfer function in the form of a phase compensator was therefore included in the feedback loop for stabilization. The differential equation defining the transfer function for this feedback element is given by:

$$\ddot{z}_{s_i} + U_1\dot{z}_{s_i} + U_2 z_{s_i} - \ddot{z}_{f_i} + U_3\dot{z}_{f_i} + U_2 z_{f_i} = 0 \qquad (8)$$

direct force feedback loop - The third feedback loop included in the feedback network is a direct feedback of the actuator force (as measured using a conventional load cell). The purpose of this feedback element is to minimize the uncertainties associated with the actual dynamics of the servo actuator. A direct result of this feedback element is that the "effective" gain of the servo actuator, as applied to only the primary and secondary feedback loops ($\epsilon_{C_i} + \epsilon_{\Delta F_i}$), can approach but never exceed unity.

Servo actuator - The servo actuator is assumed to be conventional and describable using a simple gain, G_s, and a first order lag:

$$p_2\dot{F}_i + p_1 F_i = G_s\,\epsilon_i = G_s\,(\epsilon_{\Delta F_i} + \epsilon_{C_i} + \epsilon_{F_i}) \qquad (9)$$

which can be rewritten in the following form by directly including the force feedback loop error signal, ϵ_{F_i} ($= -p_3 F_i$):

$$p_2\dot{F}_i + (p_1 + G_s p_3)\,F_i = G_s(\epsilon_{\Delta F_i} + \epsilon_{C_i}) \qquad (10)$$

It can thus be seen that the effective gain for the primary and secondary feedback loops is given by [$G_s/(p_1+G_s p_3)$], which for positive constants and unit p_1 is limited to values less than unity.

2.3 Scaling Considerations

scaling of the rotor - For a complete aeroelastic modeling of the rotor four basic scaling considerations must be met relating to the proper interactions of the aerodynamic, elastic, inertial and gravity forces (Ref. 6). Assuming complete geometric modeling, these interactions can be stated mathematically in terms of the following nondimensional parameters, which should be maintained invariant:

frequency scaling:	$\frac{E}{m\Omega^2}$	Lock number:	$\frac{\rho a c R^4}{I_b}$
advance ratio:	$\frac{V}{\Omega R}$	Froude number:	$\frac{\Omega^2 R}{g}$

The **frequency scaling parameter** insures that the blade has the correct natural frequencies in bending in relationship to rotor freqency. The **Lock number** insures that the rotor has the correct aerodynamic damping and aerodynamic coupling characteristics, and the **advance ratio** insures that the scaling of forward flight speed is correct in relationship to rotor rotational speed. The **Froude number** insures that the gravity effects, in terms of gravity springs and the rotor thrust are properly scaled in relation to the other three basic forces.

The Froude number is typically in the order of 500 to 700 and becomes increasingly important with rotor size. Because the Froude number is relatively large compared with the other nondimensional parameters strict scaling of the gravitational terms can sometimes be relaxed if their effects (as they relate to the phenomenon at hand) can be approximated.

scaling of the pylon - For the model pylon to be properly scaled relative to the rotor it must present to the rotor a properly scaled impedance. This can be achieved by matching: (1) the mass ratios between the rotor mass and that of the pylon, (2) any couplings existing between the hub degrees-of-freedom, and (3) the pylon natural frequencies (as nondimensionalized by the rotor frequency).

mass ratios:

Inspection of the air resonance equations shows that the mass ratios of importance to the air resonance instability phenomenon are those involving: (1) rotor inplane mode generalized mass and inplane pylon effective mass, Λ_3, and (2) rotor flapping mode generalized mass to pylon inertia (rotational, about some focal point, z_{foc}), Λ_4:

$$\Lambda_3 = \frac{b\, S_{48}^2}{2\, M_{eff}\, S_{49}} \quad ; \tag{11}$$

= generalized ground resonance coupling parameter, (see Ref. 7)

$$\Lambda_4 = \frac{b\, S_{12}^2}{2\, I_{eff}\, S_{10}} \qquad (12)$$

where the integrals, S_{10}, S_{12}, S_{48} and S_{49} are respectively given by:

$$S_{10} = R^2 \int_0^R m' \gamma_w^2 dr \; ; \qquad S_{12} = R \int_0^R m' r \gamma_w dr$$

$$S_{48} = R \int_0^R m' \gamma_v dr \; ; \qquad S_{49} = R^2 \int_0^R m' \gamma_v^2 dr \qquad (13a\text{-}d)$$

couplings:

Couplings of the pylon degrees-of-freedom can occur because of longitudinal center-of-gravity locations off the rotor rotation axis and because of the focusing of the roll and pitch rotations about some position below the rotor plane. A reasonable approximation to the free-flight condition is to take the focal point to be that point on the rotor rotation axis which intersects the horizontal plane containing the total aircraft center-of-gravity. Indeed, it can be seen that only for a scaling of the focal point at the aircraft center-of-gravity, do the above mass ratios, Λ_3 and Λ_4, scale commensurately. The choice of the aircraft c.g. as the focusing point is convenient because it eliminates the gravity forces as contributors to the roll and pitch spring rates and thereby minimizes the effects of a non-Froude scaling.

pylon natural frequencies:

The requirement to match the pylon impedance also requires that the natural frequencies (with respect to rotor rotational frequency) of the pylon (with the constraint of it being focused at a point, z_{foc}, below the hub), must be maintained. In the present context, this scaling principle becomes important when we wish to alter the unscaled properties of the bare rotor rig to appropriate ones which are suitably scaled.

Thus, with Eqs. (11) and (12) given above, the appropriate inertias can be determined for calculating the matrices needed for the incremental force primary feedback loops, Eq. (5). The appropriate stiffnesses for this loop can be then calculated using the constancy of nondimensional pylon frequency criterion. Thus, for two model configurations which have the same effective masses (and/or) inertias the frequency criterion then becomes that of maintaining the same effective stiffnesses.

The pylon stiffnesses in pitch and roll can each be approximated as a sum of an explicit spring rate (around the focal point), K_p, and an implicit one due to rotor flapping flexibilty, K_r. Furthermore, the rotor flapping spring rate can be conveniently expressed as a factor, $\bar{K}_r$, multiplying the rotor speed squared. This factor is frequency dependent and proportional to the number of blades and the above defined blade integration constant, S_{12}. The $\bar{K}_r$ factor depends principally on Lock number, γ , the nondimensional frequency of vibration, $\bar{\omega}$, and the blade flapping natural frequency, $\bar{\omega}_w$:

$$K_r = \Omega^2 \bar{K}_r \left(\frac{b}{2} S_{12} , \gamma , \bar{\omega} , \bar{\omega}_w \right) \tag{14}$$

Then, the invariancy of pylon frequency criterion can be written as:

$$\frac{(K_p + \bar{K}_r \Omega^2)}{I_{eff} \Omega^2} = \text{invariant} \tag{15}$$

But, I_{eff} equals $M_{eff}\, z_{foc}^2$ and M_{eff} is also invariant. Therefore, for two different configurations which must both present the same impedance to the rotor:

$$\left[\frac{K_p/\Omega^2 + \bar{K}_r}{z_{foc}^2} \right]_1 = \left[\frac{K_p/\Omega^2 + \bar{K}_r}{z_{foc}^2} \right]_2 \tag{16}$$

Noting that K_r is the same for both configurations, we can then rewrite the expression to separate out the explicit stiffness rate for the second pylon:

$$K_{p_2} = \Omega_2^2 \left\{ \left[\frac{z_{foc\ 2}}{z_{foc\ 1}} \right]^2 \frac{K_{p1}}{\Omega_1^2} + \bar{K}_r \left[\left[\frac{z_{foc\ 2}}{z_{foc\ 1}} \right]^2 - 1 \right] \right\} \tag{17}$$

It is readily apparent that, for $\Omega_1 = \Omega_2$ and $z_{foc_1} = z_{foc_2}$, the two explicit stiffnesses are equal.

2.4 Eigenanalysis

All the above formulations can be combined into a matrix eigenvalue analysis of varying size depending on the extent of the dynamics which is being considered. The initial form of this matrix equation is quadratic in the system eigenvalue, λ:

$$\left[[M]\ \lambda^2 + [C]\ \lambda + [K] \right] \left\{ \hat{Z} \right\} \tag{18}$$

where the eigenvector, $\{\hat{Z}\}$, is comprised of up to five subvectors depending on the extent of the complement of dynamic subsystems utilized:

$$\{Z_1\} = \begin{Bmatrix} \theta_{xF} \\ \theta_{yF} \\ z_{F/R} \\ \epsilon_x \\ \epsilon_y \\ \theta_{xR} \\ \theta_{yR} \end{Bmatrix}; \quad \{Z_2\} = \begin{Bmatrix} z_s^{(1)} \\ z_s^{(2)} \\ z_s^{(3)} \end{Bmatrix}; \quad \{Z_3\} = \begin{Bmatrix} z_f^{(1)} \\ z_f^{(2)} \\ z_f^{(3)} \end{Bmatrix};$$

$$\{Z_4\} = \begin{Bmatrix} F^{(1)} \\ F^{(2)} \\ F^{(3)} \end{Bmatrix}; \quad \{Z_5\} = \begin{Bmatrix} \epsilon_1^{(1)} \\ \epsilon_1^{(2)} \\ \epsilon_1^{(3)} \end{Bmatrix} \tag{19a-e}$$

where: $$\epsilon_1^{(i)} = \int_0^t z_s^{(i)}\, dt; \quad i = \text{actuator number} \tag{20}$$

Because some of the subsystem dynamics lack second order differentiated terms it can be appreciated that the "mass" matrix, [M], as depicted above is singular. Consequently, in order to remove this singularity and to reduce the eigenproblem to a more tractable form an augmented state vector is formed. The resulting matrix eigenproblem is then given by:

$$\left[\lambda\ [B] - [A] \right] \left\{ Y \right\} \tag{21}$$

where:

$$\left[Y \right] = \left[\dot{Z}_1,\ \dot{Z}_2,\ \dot{Z}_3,\ Z_1,\ Z_2,\ Z_3,\ Z_4,\ Z_5 \right] \tag{22}$$

The semi-canonical form of the matrix eigenalysis, as represented by Eq. (21), taken together with standard eigenvalue computational routines, were used to extract the required eigenvalues.

3. Numerical Results

3.1 Selection of Test Case Configurations

The objectives of the study were met by considering configurations of increasing complexity beginning with a realistic full scale free-flying helicopter (see Table 1, below). Subsequent cases represent various model configurations scaled with a geometric scale factor of 1/5.727. For a strict Froude scaling (Cases 2a and 2b) the velocity scale factor must be and is 1/2.393. For all the remaining cases a mixed scaling scheme was used wherein the velocity scale factor was 1/1.726. These subsequent cases were analyzed with the inclusion of ever increasing constraints and/or dynamic subsystems. The following table identifies and describes the cases analyzed in the study:

Table 1. Schedule of Scaled Configurations Analyzed

Case	Model Scaling	Pylon Type	Active Control	Flight Type	Λ_{3_φ}	Λ_{4_φ}
1	FS	actual AC	N	free flight	-	-
2a	Froude	" "	N	" "	-	-
2b	"	" "	N	constrained	0.0312	0.3780
3a	mixed	" "	N	free flight	-	-
3b	"	" "	N	constrained	0.0312	0.3780
3c	mixed, (100% C_T/σ)	" "	N	"	0.0312	0.3780
4	"	actual rig	N	"	0.0210	0.1787
5a	"	modified rig	Y(1)*	"	0.0312	0.3780
5b	"	" "	Y(1, 3), ($p_3>0$)	"	0.0312	0.3780
5c	"	actual rig	Y(1)	"	0.0312	0.2654
5d	"	" "	Y(1), ($p_2>0$)	"	0.0312	0.2654
5e	"	" "	Y(1, 2), ($p_2=0$)	"	0.0312	0.2654

* (indicates which feedback loops are activated)

For all cases the Lock number was the same value (= 7.2394) and the air resonance instability mode was the predominantly roll mode.

Note that in Case 4 the actual test rig pylon parameters (with the active controller disengaged) are quite different than the appropriately mass-scaled parameters of the actual aircraft. This is evident from the dissimilarity of the Λ_{3_φ} and Λ_{4_θ} values compared with those for all the other cases. Although these parameters, (as defined in the roll direction) are the most pertinent to the air resonance phenomenon, the similarly defined pitch direction parameters show even greater dissimilarity. The Case 4 configuration is one with practically isotropic properties as contrasted with all the other configura-

tions, which have significant anisotropy (either actual or simulated).

In cases 5a thru 5d the network parameters for the active controller were selected to give approximately scaled pylon parameters. Case 5a represents the case wherein the focus point was artificially set at the properly scaled value to represent the actual aircraft c.g. point (cases 1 and 2). All other group 5 cases used the actual test rig focal point which was somewhat lower than the accurately scaled one and thereby introduced some coupling error.

The aeromechanical properties of the rotor and pylons considered (both full scale airframe and the actual air resonance test rig) are given in Table 2:

Table 2. Aeromechanical Properties of Rotor and Pylons used in Numerical Examples

1.	Rotor (full scale) properties		
	(Nominal) tip speed, ΩR	220.98	m/s
	Froude number @ nom ΩR	608.34	
	Radius, R	8.179	m
	(Average) mass distribution, m'	6.994	kg/m
	Total rotor mass, m_R	558.8	kg
	Flatwise bending frequency, ω_w, @ nom ΩR	1.1	/rev
	Edgewise bending frequency, ω_v, @ nom ΩR	0.75	/rev
	Modal damping for bending modes, ζ_v, ζ_w	0.01	
	Number of blades	4	
2.	Full scale pylon (fuselage) properties		
	Mass, m_F	6949.0	kg
	Roll moment of inertia, I_φ	6926.0	kg m^2
	Pitch moment of inertia, I_θ	53,554.8	kg m^2
	vertical c.g. position, h_i	1.8593	m
	longitudinal c.g. position, x_{CG}	-0.0914	m
3.	model scale pylon (actual rig) properties		
	Mass, m_F	10.88	kg
	Roll moment of inertia, I_φ	3.6065	kg m^2
	Pitch moment of inertia, I_θ	3.0777	kg m^2
	vertical c.g. position, h_i	0.3048	m
	longitudinal c.g. position, x_{CG}	0.0	m
4.	Supplementary rotor properties		
	Lock number, γ	7.2394	
	(Froude scaled) C_T/σ	0.0609	
	(Average, full scale) chord, c	0.6282	m
	Precone angle, β_B	3.0	deg
	(Average) lift curve slope, a	0.1	/deg
	c_{do}	0.01	

For those cases wherein the active control feedback loops were activated (Cases 5a thru 5e), appropriate values of the $[\Delta M]$, $[\Delta C]$ and $[\Delta K]$ matrices were generated according to the following scheme:

(1) Values of the inplane mass coupling parameters, Λ_{3_θ} and Λ_{3_φ}, in pitch and roll, as determined from the Case 2b parameters, were first calculated.

(2) Using these values of the mass coupling parameters the required (simulated) effective masses in pitch and roll were calculated for the case considered. The inertias about the gimbal could then be found using the actual focal distance, z_{foc}.

(3) Using the calculation for rotor stiffness, K_r, and the different values of focal distances for Case 2b and the case considered, the equivalent explicit pylon spring rates in pitch and roll, K_{p_θ} and K_{p_φ}, respectively, were calculated using Eq. (17).

(4) The Δ matrices were then calculated subtracting the actual rig parameters from the simulation required ones as calculated using the above steps (1) thru (3).

3.2 Trim Cases

In order to more completely compare the effects of mixed scaling, especially in forward flight, the various configurations defined in Table 1 were used to calculate trim configurations. For this purpose a simple trim calculation program, based on the simplified aerodynamic strip theory of Ref. 8, was used. These trim calculations were nominally made subject to the conditions of a required thrust equal to the configuration gross weight, a required forward flight speed based on a given advance ratio and the appropriate rotor speed, and a required propulsive force. This propulsive force was based on the scaling of the assumed value of (full scale) fuselage equivalent flat plate area, f, of 1.914 m^2.

Because of the difference of speed scaling between Cases 1 and 2 (a&b) and all the remainder cases, the matching of total configuration gross weight led to different values of C_T/σ for the same scaled values of thrust. Consequently, as shown in Table 1, for Cases 3c and beyond the same collective angles and inflow ratios as for Cases 1 and 2 (a&b) were used so as to achieve a scaling on C_T/σ. Note that for these conditions the rotor is "overthrusting" relative to the scaled required gross weight. For a gimbaled configuration with the capability to null out the steady load, this situation can be readily accommodated.

3.3 Results for Cases with only Passive Pylon Characteristics

Using Table 1 as a guide, one can interpret the eigenvalue results presented in Figures 5 and 6 for the passive pylon characteristics cases. Figure 5 presents the hovering case results for Cases 1, 2(a&b), 3(a-c) and 4, for ±20% variations in the

(nondimensional) appropriately scaled nominal values of rotor speed. Figure 6 presents the eigenvalue results for variations in advance ratio for the same cases as shown in Fig. 5:

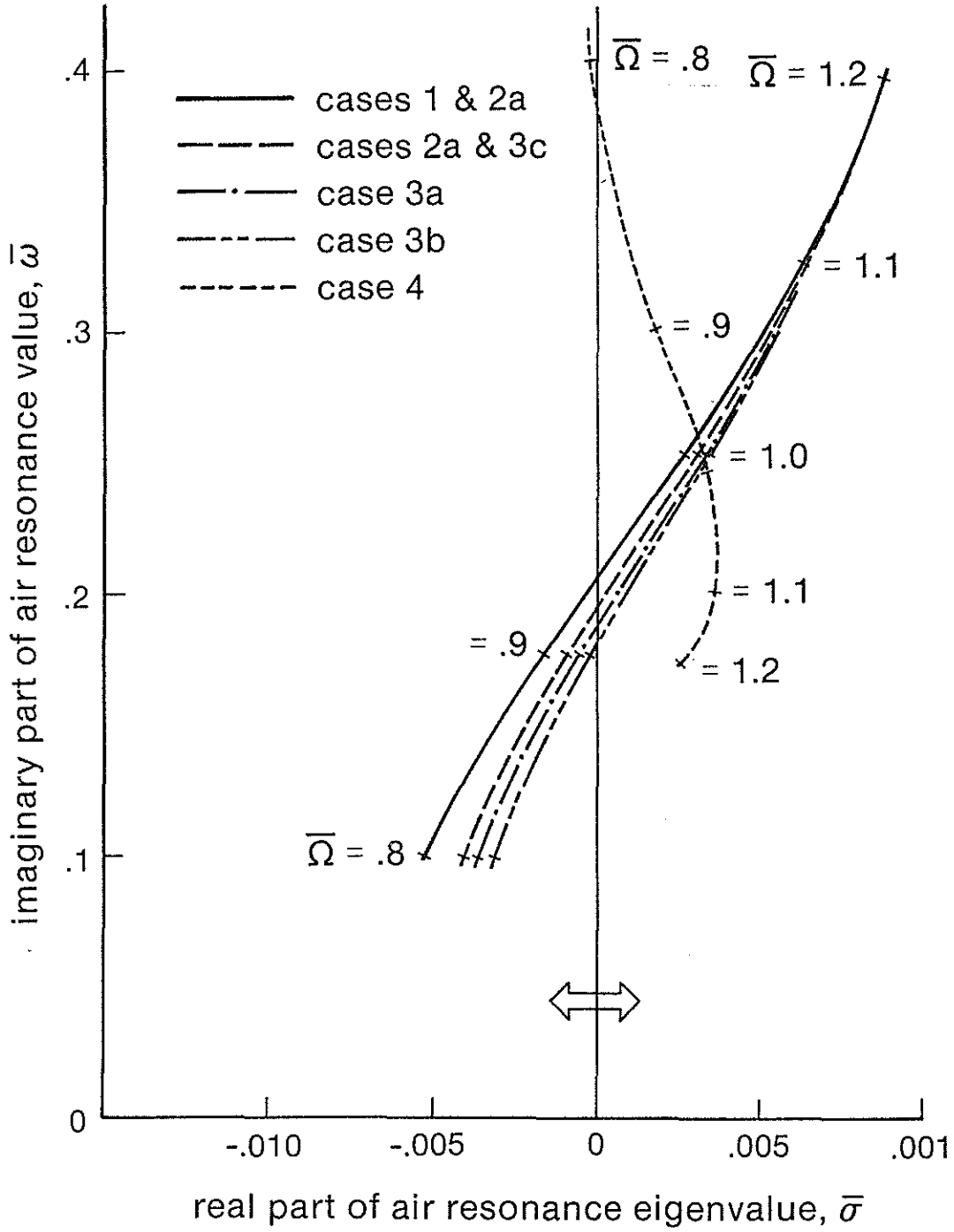

Figure 5. Root Locus Diagrams of the Air Resonance Eigenvalues for Variations in Rotor Speed, Hovering Conditions, Passive Pylon Cases

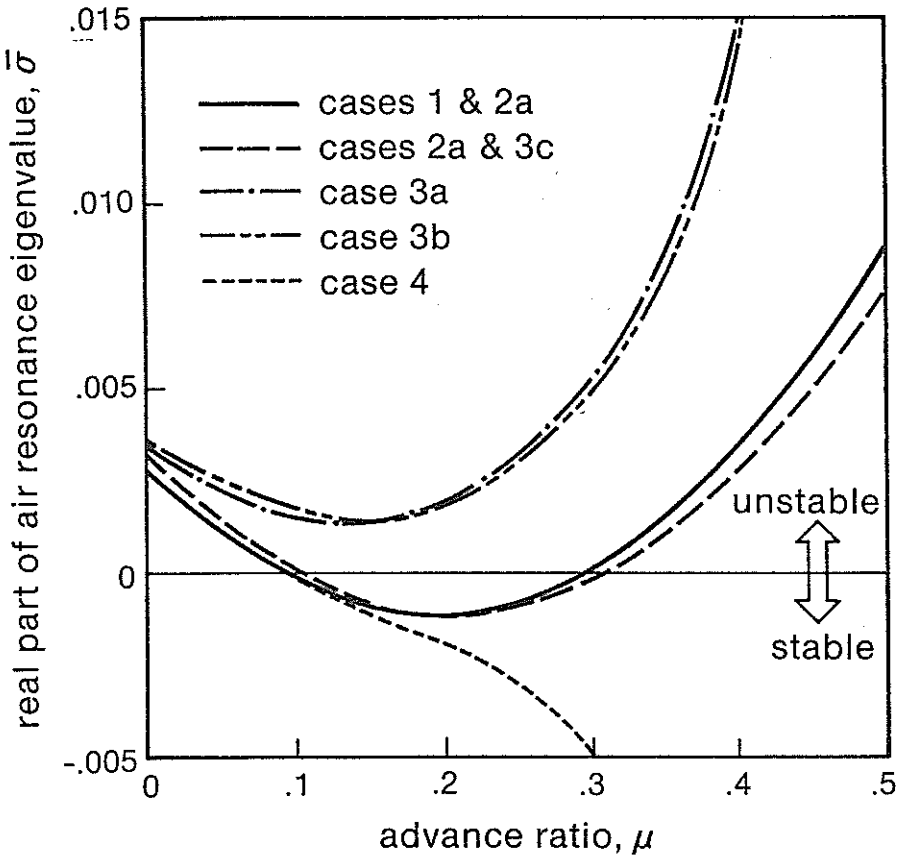

Figure 6. Variation of Air Resonance Stability Characteristics with Advance Ratio, Passive Pylon Cases

The following interpretations can be drawn from these figures:

(1) Comparison of the Case 2a and 2b results shows that a penalty in accuracy is paid for applying the gimbal constraint. In this case the constraint has reduced the accuracy of the real part of the eigenvalue by approximately 13%. This penalty cannot be easily overcome by the potential use of the active control capability because this constraint impacts on the generation of rotor blade airloads as well as pylon inertial loads, as discussed above.

(2) The use of a non-Froude scaling together with a matching of the rotor thrust to the configuration scaled gross weight leads to further inaccuracies. However, the use of a scaled blade loading (Case 3c) leads to a retrieval of the Froude scaled (but still constrained) results. Thus, the gimbal-constrained, Froude scaled characteristics are achievable with this form of scaling.

(3) The air resonance stability characteristics of the actual test rig pylon appear to be completely dissimilar to those of the pylon which are to be modeled despite the relative closeness of results at the nominal rotor speed. Indeed, as inspection of the eigenvectors (coupled mode shapes) showed, the instabilities obtained for Cases 1, 2(a&b) and 3(a-c) were all predominantly roll modes whereas those obtained for Case 4 were predominantly circular whirl modes.

3.4 Results for Cases with Active Pylon Characteristics

The results obtained for various combinations of active pylon feedback loops are presented in Figures 7 and 8:

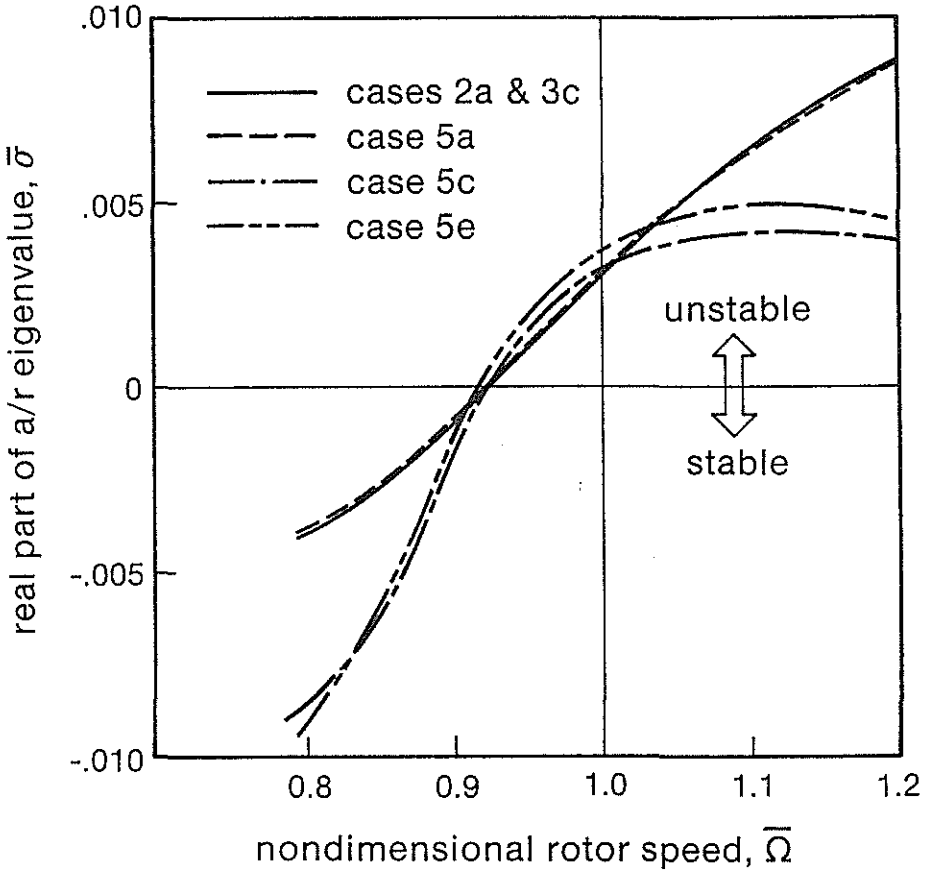

Figure 7. Variation of Air Resonance Stability Characteristics with Rotor Speed, Active Pylon Cases

From the results of Figure 7 the following interpretations can be made:

(1) Comparison of the results of Cases 2a (and 3c) with those of Case 5a shows that with the use of active control of the pylon characteristics the air resonance dynamics can be well duplicated despite the use of a non-Froude scaling, provided the focal distance is accurately scaled.

(2) With the use of a primary feedback scheme wherein the Λ_{3_θ} and Λ_{3_φ} mass ratio parameters are maintained equal, reasonably similar results can be obtained despite the fact that the Λ_4 mass ratio parameters are not equal. Note that the Case 5c and 5e results correlate poorly with those of Case 5a for conditions removed from the nominal rotor speed despite the good correlation at the nominal rotor speed. This poor performance is most likely due to the fact that the same value of K_r was used throughout despite the fact that this characteristic is frequency dependent. Refinement of the use of the rotor stiffness would be expected to improve the correlation significantly.

(3) The incorporation of both the primary and secondary feedback loops (Case 5e) shows the stability characteristics to be somewhat deviated from the target characteristics defined by Case 5a and 5c at the nominal rotor speed, and again poorly correlated for conditions off the nominal rotor speed. The same interpretation as given above applies to this case as well. The Case 5e results must furthermore be deemed preliminary at this point since a great deal of parameter variation is yet to be made in obtaining a completely optimal sizing of the various coefficients in the position controller feedback loop.

The remaining parameter variations made in the present study relate to the force feedback loop and to the servo actuator. The effect of this feedback loop was assessed by varying the p_3 parameter over three orders of magnitude. The results of this variation are presented in Figure 8. The figure shows that the effects of this feedback loop are generally benign. Except for wide excursions in the stability parameter for large values of the p_3 parameter, the air resonance characteristics are not significantly. It would appear that a reasonable value of gain for this feedback would be approximately 0.65.

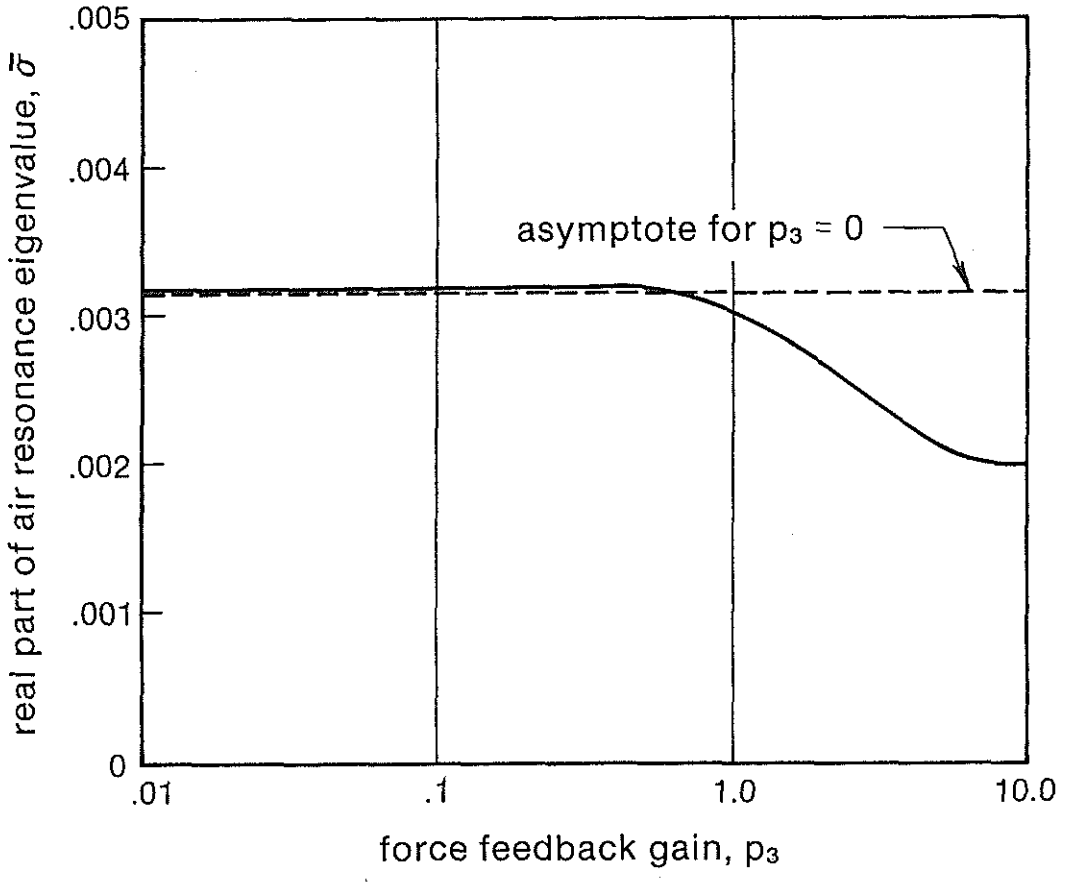

Figure 8. Variation of the Air Resonance Characteristics with Force Feedback Gain, Scaled Focal Location, Hovering Flight Condition

Since all servo actuators have a roll-off of performance at some high frequency, the assumption of a first order lag idealization of the servo actuators is a reasonable one. Moreover, it is reasonable to expect that a parametric variation of this first order lag time constant, p_2, would be appropriate and instructive. Unfortunately, the reduction of the p_2 parameters to very small values constitutes a singular perturbation problem. The matrix eigenvalue solution technique used proved to be incapable of extracting accurate roots for matrices with arbitrarily small diagonal terms. It is reasonable to expect that, in practice, the value of this parameter should be kept low enough to ensure a relatively high corner frequency ($1/p_2$) so that there would be minimum phase lag at all the system frequencies, especially that of the air resonance mode.

4.0 Concluding Remarks

The use of active control of pylon dynamic properties as a means for "tailoring " the effective impedance the pylon presents to the rotor in a potential air resonance prone environment represents an improvement over traditional methods for the testing of this type of helicopter rotor-fuselage coupled instability. Specific advantages of this method are:

(1) It offers considerably more variability in the range of pylon parameters which can be modeled in a gimbal mounted pylon configuration.

(2) It inherently provides a practical means for effecting a centering of the gimbal to take out the trim loads.

(3) It offers a relaxation of the usual gimbal constraint in that the vertical degree-of-freedom is now automatically included.

(4) It provides a means for removing the parasitic damping and stiffness inherently present in gimbal mounted configurations.

On the basis of the results presented the following specific conclusions have been drawn:

(1) The inaccuracies posed by the gimbal constraint are not large for the actual configuration examined, but are still not addressed by this type of testing.

(2) The use of a non-Froude scaling is practical for air resonance testing provided that: (a) the nondimensional blade loading (C_T/σ) and advance ratio (μ) are maintained unchanged, (b) the inplane mass ratio parameter is maintained unchanged (using the incremental force feedback capablility) and (c) the explicit gimbal spring rates are sized to produce the correct (nondimensional) roll and pitch frequencies.

(3) The use of an accurate geometric scaling of the vertical gimbal location would enhance the accuracy of this type of testing. This accuracy enhancement would occur in part by virtue of the elimination of the need for calculating the implicit rotor pitch and roll spring rates provided by the rotor blades in bending, and in part by the assurance of having the correct mix of inplane and out-of-plane bending in the air resonance responses.

(4) The correct tailoring of the roll and pitch spring rates is heavily dependent on the use of analysis for detemining the effective rotor pitch and roll spring rates. This analytic task introduces a dependence of the experiment on analysis which must result in the dilution of the experimental accuracy.

(5) The use of the force feedback loop, while not producing any overt inaccuracy contributes little to the accuracy of this method of testing and elimination of this feedback should be considered.

Acknowledgements - The author wishes to acknowledge the sponsorship of this work by the Sikorsky Aircraft Division of United Technologies Corporation and, in particular, to thank Messrs. C. Niebanck and R. Goodman of Sikorsky for their support and useful contributions. This work was also performed under the aegis of the U.S. Army Research Office.

6.0 Notation

a	Airfoil section lift curve slope, 1/deg
b	Number of blades
C_T/σ	Rotor thrust coefficient per blade solidity
c	Blade chord, cm
c_{d_o}	Airfoil section minimum drag coefficient
c_f	Pylon effective translational damping at hub, N-s/m
EI	Blade bending stiffness, N-m^2
F_{x_f}, F_{y_f}	Hub force excitations, x- and y-directions, respectively, N
G_s	Servo actuator gain
g	Gravitational acceleration, m/sec^2
h_1	Distance airframe c.g. is below rotor hub, m
I_b	Blade flapping inertia, Kgm^2
I_{eff}	Effective pylon + rotor inertia about focal point, Kgm^2
I_{θ_f}, I_{ϕ_f}	Airframe pitch and roll inertias, respectively, about airframe c.g., Kgm^2
K_a	Aerodynamic effectivity, Kg-m
K_p	Spring rate for explicit spring about focal point, N-m
K_r	Equivalent spring rate for pylon stiffening in pitch and/or roll due to rotor flexibility, N-m
[M], [C], [K]	Inertia, damping and stiffness matrices, respectively
M_{eff}	Effective (total) mass at hub in inplane directions, kg
M_{x_f}, M_{y_f}	Hub moment excitations in roll and pitch, respectively, N-m
m_f	Airframe (pylon) mass, Kg
m_R	Rotor mass, kg
m'	Blade mass distribution, Kg/m
m'_o	Reference blade mass distribution, kg/m
p, pa, pb	Constants defining position controller dynamics, N
P_1, P_2, P_3	Constants defining servo actuator force dynamics
Q_1, Q_2, Q_3	Constants defining low pass filter dynamics
R	Rotor radius, m
r	Blade spanwise variable, m
$S_{10}, \ldots S_{49}$	Blade mass modal integration constants
T	Rotor thrust, N
$T_1, \ldots T_{25}$	Blade aerodynamic modal integration constants
$[T_1]$, $[T_2]$	Force and deflection resolution matrices for hub to actuator attachment degrees-of-freedom

U_1, U_2, U_3	Constants defining phase compensator dynamics
V	Forward flight speed, m/sec
x_a, y_a	longitudinal and lateral actuator attachment point locations from rotor axis, respectively, m
x_F, y_F, z_F	Longitudinal, lateral and vertical hub displacements, respectively, m
z_{foc}	pivot or focal point of pylon below hub, m
z_1, z_2, z_3	vertical deflections of actuator attachment points, m
z_{s_i}, z_{f_i}	Output signals from i'th phase compensator and low-pass filters, respectively
β_B	Blade precone angle, deg
γ	Blade Lock number
γ_v, γ_w	Blade 1st edgewise and flatwise mode shapes, respectively
ϵ_x, ϵ_y	Cyclic rotor mode descriptions of blade edgewise bending in longitudinal and lateral directions, respectively
ϵ_1, ϵ_2, ϵ_3	Error inputs to servo actuators, N
ζ_v, ζ_w	Blade structural equivalent critical damping ratios for edgewise and flatwise bending, respectively
η	Factor to account for flight configuration
θ_{x_F} θ_{y_F}	Hub roll and pitch motion, respectively, deg
θ_{x_R}, θ_{y_R}	Cyclic rotor mode descriptions of blade flatwise bending in roll and pitch directions, respectively
Λ_3, Λ_4	Inplane and rotational coupling parameters, respectively
λ	System eigenvalue ($= \sigma \pm i\omega$), 1/sec
λ_ℓ	Geometric scale factor
λ_V	Velocity scale factor
μ	Rotor advance ratio
ρ	Air density, kg/m^3
σ	Real part of system eigenvalue, giving stability information, 1/sec
Ω	Rotor speed, rad/sec
Ω_{ref}	(Reference) or nominal rotor speed, rad/sec
ω	Imaginary part of eigenvalue, giving coupled frequency information, rad/sec
ω_v, ω_w	Inplane and flapwise (first) natural frequencies, respectively, of rotating elastic blade, rad/sec

Superscripts

$(\ )^{(a)}$	Relates to aerodynamic forces
$(\ )^{(h)}$	Relates to (hydraulic) actuator forces
$(\ )^{(i)}$	Pertaining to i'th servo actuator or feedback network
$(\bar{\ })$	Nondimensionalization with respect to appropriate combinations of R, m_o' and/or Ω_{ref}

Subscripts

$(\ )_{\Delta F}$	Relating to the primary (incremental force) feedback loop
$(\ )_C$	Relating to the secondary (position controller) feedback loop
$(\ )_\theta$	Pertaining to quantities measured about focal point in pitch (θ_y rotational sense)
$(\ )_\varphi$	Pertaining to quantities measured about focal point in roll (θ_x rotational sense)

7.0 References

1. C. Chen, J. Staley — Flight Evaluation of Loads and Stability Characteristics of a Bearingless Main Rotor - 1/5.86 Froude Scale Model Test Results. Boeing Vertol Co. Report D210-11245-1. (1977).

2. W.H. Weller, R.L. Peterson — Inplane Stability Characteristics for an Advanced Bearingless Main Rotor Model. J. of the American Helicopter Society. (1984) 29 (3) 45-53.

3. R.L. Bielawa — An Improved Technique for Testing Helicopter Rotor-Pylon Aeromechanical Stability Using Rotor Dynamic Impedance Characteristics. Vertica (1985) 9 (2) 181-197.

4. R.L. Bielawa — Notes Regarding Fundamental Understandings of Rotorcraft Aeroelastic Instability. Proceedings of the 11th European Rotorcraft Forum (1985) paper no. 62.

5. K. Ogata — Modern Control Engineering. Prentice-Hall, Inc., Englewood Cliffs, N.J. (1970).

6. G.K. Hunt — Similarity Requirements for Aeroelastic Models of Helicopter Rotors. Aeronautical Research Council C.P. no. 1245 (1973).

7. R.P. Coleman, A.M. Feingold — Theory of Self-Excited Mechanical Oscillations of Helicopter Rotors with Hinged Blades. NACA Report 1351 (1958).

8. A. Gessow, G.C. Myers — Aerodynamics of the Helicopter. Frederick Ungar Co., New York, N.Y. (1952).

Appendix A - Inclusion of Heave Degree-of-Freedom in Air Resonance Dynamic Equations

The simplified equations of motion used as the basis for this study are those presented in Ref. 4. This equation set is intended as an approximate, but reasonably representative analysis of the air resonance phenomenon and is not intended for general analysis applications in support of actual helicopter design efforts. The modifications required for the dynamic equations relate to the inclusion of the fuselage (hub) heave degree-of-freedom, z_F, the addition of rudimentary quasi-static (forward flight) aerodynamics, and the inclusion of the explicit servo actuator forces, F_i, (i= 1, 2, 3). As in Ref. 4, the required modifications are presented without formal

mathematical development. A full presentation of the details of the modified quasi-static aerodynamics is beyond the scope of this paper; only the bases of the formulation are presented.

Elasto-mechanics

The pylon substructure is now defined in terms of the five rigid body degrees-of-freedom of the hub: longitudinal, lateral and vertical translations and pitch and roll rotations. The nine resulting differential equations respectively model the responses in hub x-, y- and z- translations, hub roll and pitch rotations, blade cyclic inplane (edgewise) bending rotor modes in the x- and y- directions, and blade cyclic flapwise (flatwise) bending rotor modes in the roll and pitch directions:

$$\{Z\}^T = \{x_F/R,\ y_F/R,\ z_F/R,\ \theta_{x_F},\ \theta_{y_F},\ \epsilon_x,\ \epsilon_y,\ \theta_{x_R},\ \theta_{y_R}\}^T \qquad (A.1)$$

The additional elasto-mechanical portions of the equations due to the heave degree-of-freedom and the explicit actuator forces only are presented in the equations to follow. Repetition of the basic presentation of Ref. 4 is ommitted for brevity.

Hub Longitudinal Force (F_x)

(only detailed changes in perturb. airloads), $\Delta F_x^{(a)}$

Hub Lateral Force (F_y)

(only detailed changes in perturb. airloads), $\Delta F_y^{(a)}$

Hub Vertical Force (F_z)

$$(m_{F_z} + m_R)\,\ddot{z} - m_{F_z} x_{CG}\,\ddot{\theta}_{y_F} + \eta(m_{F_z} + m_R)\,V\dot{\theta}_{y_F} = F_z^{(a)} + F_z^{(h)} \qquad (A.2)$$

Hub Roll Moment (M_{x_F})

$$\ldots = \ldots + \Delta M_{x_F}^{(a)} + M_{x_F}^{(h)} \qquad (A.3)$$

Hub Pitch Moment (M_{y_F})

$$\ldots - m_F x_{CG}(\ddot{z}_F + \eta V\dot{\theta}_{y_F}) = \ldots + \Delta M^{(a)}_{y_F} + M^{(h)}_{y_F} \qquad (A.4)$$

Rotor Longitudinal Edgewise Excitation (z_{ϵ_x})

(only detailed changes in perturb. airloads), $\Delta z^{(a)}_{\epsilon_x}$

Rotor Lateral Edgewise Excitation (z_{ϵ_y})

(only detailed changes in perturb. airloads), $\Delta z^{(a)}_{\epsilon_y}$

Rotor Rollwise Flatwise Excitation ($z_{\theta_{x_R}}$)

(only detailed changes in perturb. airloads), $\Delta z^{(a)}_{\theta_{x_R}}$

Rotor Pitchwise Flatwise Excitation ($z_{\theta_{y_R}}$)

(only detailed changes in perturb. airloads), $\Delta z^{(a)}_{\theta_{y_R}}$

where: η = 1, (or) 0., depending upon whether the pylon (fuselage) is, respectively, in a free-flight (or) gimbaled configuration.

Quasi-static Aerodynamics

The additional aerodynamic terms in the dynamic equations (to account for the heave degree-of-freedom and for forward flight conditions) were formed using typical quasi-static aerodynamic theory. The details of the additional terms follow from the following expressions for the components of airfoil sectional velocity:

Tangential component, U_T:

$$U_T = R\left\{\Omega(\bar{r} + \mu\sin\Psi) + (\dot{y}\cos\Psi - \dot{x}\sin\Psi)/R + \gamma_v[(\dot{\epsilon}_y - \Omega\epsilon_x)\cos\Psi - (\dot{\epsilon}_x + \Omega\epsilon_y)\sin\Psi]\right\} \qquad (A.5)$$

Perpendicular component, U_P:

$$U_p = R\left\{\lambda\Omega + \gamma_w[(\dot{\theta}_{y_R} - \Omega\theta_{x_R})\cos\Psi - (\dot{\theta}_{x_R} + \Omega\theta_{y_R})\sin\Psi\,] + \bar{r}(\dot{\theta}_{y_F}\cos\Psi - \dot{\theta}_{x_F}\sin\Psi) + \beta_B(\dot{x}\cos\Psi + \dot{y}\sin\Psi)/R + \Omega\mu\left[(1-\eta)\theta_{y_F} + [\,\beta_B + \gamma_w'(\theta_{x_R}\sin\Psi - \theta_{y_R}\sin\Psi\,]\right] - \dot{z}_F/R\right\} \tag{A.6}$$

Appendix B - Approximation to Implicit Angular Pylon Spring due to Rotor Elastic Flapping

An approximation to the implicit angular pylon stiffness afforded by the flexible rotor can be obtained from the set of dynamic equations described above in Appendix A. This spring rate is taken to be the rotor moment 180° out-of-phase with pylon motion which results when the pylon is undergoing sinusoidal motion at some frequency, ω. If the dynamic system is assumed to consist of only pylon rotation in one of the pylon variables, say θ_{x_F}, and the two rotor flapping degrees-of-freedom, θ_{x_R} and θ_{y_R}, then the moment exerted by the rotor on the pylon can be written using the equation for pylon rolling moment, as follows:

$$M_{\theta_F} = -(b/2)\left\{ S_{12}[\,\ddot{\theta}_{x_R} + 2\Omega\dot{\theta}_{y_R}\,] + K_a\Omega R\,[\,T_4\dot{\theta}_{x_F} + T_{11}(\dot{\theta}_{x_R} + \Omega\theta_{y_R})\,]\right\} \tag{B.1}$$

where: $K_a = \frac{1}{2}\rho a R^4$

The rotor response variables, θ_{x_R} and θ_{y_R}, are expressible as implicit functions of the pylon rotation variable, θ_{x_F}, using the dynamic equations for rollwise and pitchwise flapping, respectively:

$$S_{10}[\,\ddot{\theta}_{x_R} + \ldots - T_{13}(\dot{\theta}_{x_R} + \Omega\theta_{y_R})\} = -S_{12}\,\ddot{\theta}_{x_F} \tag{B.2.a}$$

$$S_{10}[\,\ddot{\theta}_{y_R} + \ldots - T_{13}(\dot{\theta}_{y_R} - \Omega\theta_{x_R})\} = 2\Omega S_{12}\,\dot{\theta}_{x_F} \tag{B.2.b}$$

Then, the assumption of sinusoidal motion is invoked:

$$\{\,\theta_{x_R},\ \theta_{y_R},\ \theta_{x_F}\,\}^T = \{\,\bar{\theta}_{x_R},\ \bar{\theta}_{y_R},\ \bar{\theta}_{x_F}\,\}^T e^{i\omega t} \tag{B.3}$$

This assumption then renders Eqs. (B.1) and (B.2.a&b) a soluble set of algebraic equations wherein the rotor response variables (θ_{x_R} and θ_{y_R}) can be removed to yield a single equation for the sinusoidal rotor moment, which is then linear in θ_{x_F}. The details of the substitution and subsequent removal of θ_{x_R} and θ_{y_R} from the expression are straightforward but tedious and, hence, are omitted herein for clarity. The resulting equation can then be written in the following form:

$$M_{\theta_F} = \Omega^2 (b/2) S_{12} \{F(\bar{\omega}, \bar{\omega}_w, K_a, \ldots)\} \bar{\theta}_{x_F} e^{\bar{i}\omega\Psi} \qquad (B.4)$$

$$= -\Omega^2 [\, \bar{K}_r + i\bar{\omega}\, \bar{C}_r \,] \bar{\theta}_{x_F} e^{i\bar{\omega}\Psi}$$

Thus, the required rotor spring rate is seen to be the negative real part of the resulting rotor moment. Note that the effective pylon damping is equal to the negative imaginary part divided by the frequency.